



FVCOM validation experiments: Comparisons with ROMS for three idealized barotropic test problems

Haosheng Huang,^{1,2} Changsheng Chen,¹ Geoffrey W. Cowles,¹ Clinton D. Winant,³ Robert C. Beardsley,⁴ Kate S. Hedstrom,⁵ and Dale B. Haidvogel⁶

Received 18 September 2007; revised 21 May 2008; accepted 10 June 2008; published 26 July 2008.

[1] The unstructured-grid Finite-Volume Coastal Ocean Model (FVCOM) is evaluated using three idealized benchmark test problems: the Rossby equatorial soliton, the hydraulic jump, and the three-dimensional barotropic wind-driven basin. These test cases examine the properties of numerical dispersion and damping, the performance of the nonlinear advection scheme for supercritical flow conditions, and the accuracy of the implicit vertical viscosity scheme in barotropic settings, respectively. It is demonstrated that FVCOM provides overall a second-order spatial accuracy for the vertically averaged equations (i.e., external mode), and with increasing grid resolution the model-computed solutions show a fast convergence toward the analytic solutions regardless of the particular triangulation method. Examples are provided to illustrate the ability of FVCOM to facilitate local grid refinement and speed up computation. Comparisons are also made between FVCOM and the structured-grid Regional Ocean Modeling System (ROMS) for these test cases. For the linear problem in a simple rectangular domain, i.e., the wind-driven basin case, the performance of the two models is quite similar. For the nonlinear case, such as the Rossby equatorial soliton, the second-order advection scheme used in FVCOM is almost as accurate as the fourth-order advection scheme implemented in ROMS if the horizontal resolution is relatively high. FVCOM has taken advantage of the new development in computational fluid dynamics in resolving flow problems containing discontinuities. One salient feature illustrated by the three-dimensional barotropic wind-driven basin case is that FVCOM and ROMS simulations show different responses to the refinement of grid size in the horizontal and in the vertical.

Citation: Huang, H., C. Chen, G. W. Cowles, C. D. Winant, R. C. Beardsley, K. S. Hedstrom, and D. B. Haidvogel (2008), FVCOM validation experiments: Comparisons with ROMS for three idealized barotropic test problems, *J. Geophys. Res.*, *113*, C07042, doi:10.1029/2007JC004557.

1. Introduction

[2] The finite-volume numerical method has been introduced into the ocean modeling community [Marshall *et al.*, 1997; Ward, 1999; Chen *et al.*, 2003; Cheng and Casulli, 2003]. Unlike finite-difference and finite-element methods, in a finite-volume discretization, the governing equations of

momentum, mass, and tracers are expressed by their integral forms over individual control volumes and solved numerically by flux calculation through the volume boundaries. As a result, the finite-volume approach has the advantage of intrinsically enforcing conservation laws in both individual control volumes and the entire computational domain.

[3] In principle, the finite-volume method can employ either structured rectangular grids or arbitrary unstructured grids. Unstructured triangular grids can provide an accurate geometric representation of complex coastlines and are amenable to local grid refinement as well as dynamic grid adaptation schemes. Therefore, the finite-volume ocean model employing triangular elements is a good alternative to the traditional ocean models employing structured grids and combines the advantage of finite-element methods for geometric flexibility and finite-difference methods for simple code structure and computational efficiency.

[4] An unstructured-grid, finite-volume, three-dimensional primitive equation, coastal ocean model (Finite-Volume Coastal Ocean Model (FVCOM)) was developed [Chen *et al.*, 2003, 2006, 2007; Cowles, 2008]. It has been applied to

¹School for Marine Science and Technology, University of Massachusetts Dartmouth, New Bedford, Massachusetts, USA.

²Now at Department of Oceanography and Coastal Sciences, Louisiana State University, Baton Rouge, Louisiana, USA.

³Scripps Institution of Oceanography, University of California, San Diego, La Jolla, California, USA.

⁴Department of Physical Oceanography, Woods Hole Oceanographic Institution, Woods Hole, Massachusetts, USA.

⁵Arctic Region Supercomputing Center, University of Alaska, Fairbanks, Alaska, USA.

⁶Institute of Marine and Coastal Science, Rutgers University, New Brunswick, New Jersey, USA.

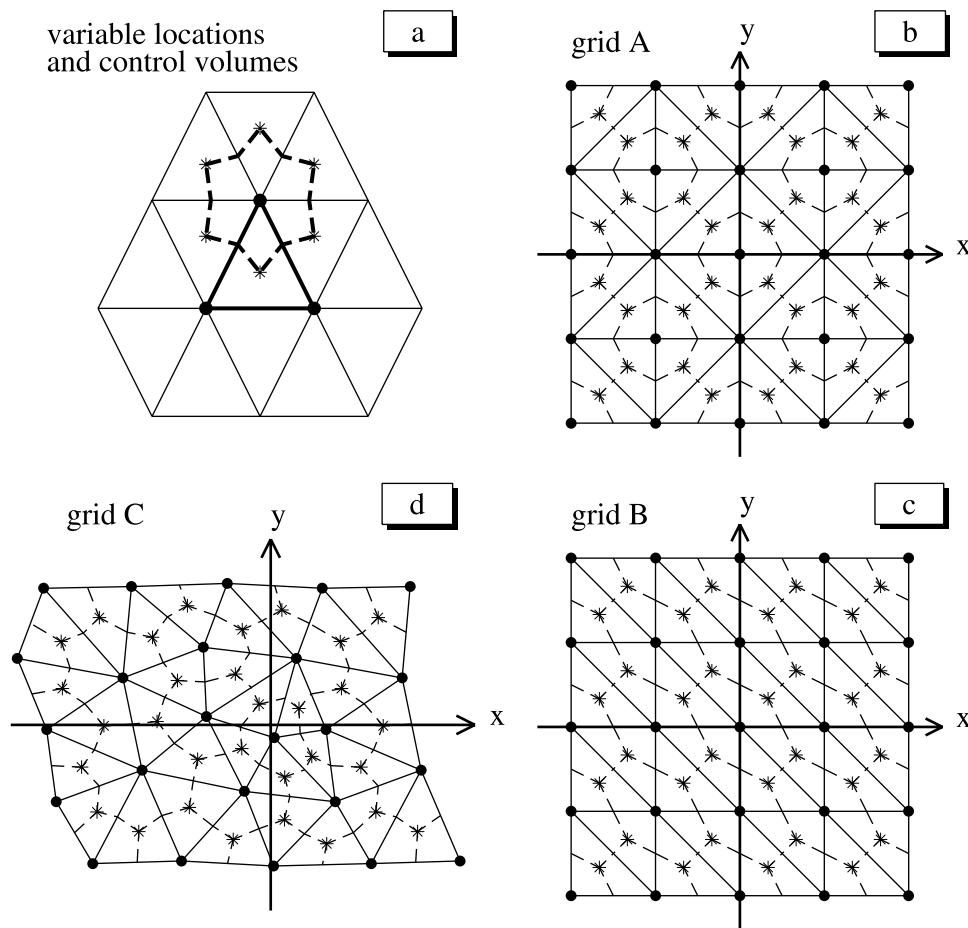


Figure 1. Illustration of the (a) FVCOM unstructured triangular grid and the three types of grid mesh: (b) grid A, (c) grid B, and (d) grid C. Variable locations: solid circles (H (undisturbed water depth)), ζ (sea surface elevation), D (total water depth), w (vertical velocity component), S (salinity), T (temperature), and asterisks (u, v (horizontal velocity components)). The solid line triangle represents the momentum control element in which u and v are calculated, and the dashed-line polygon represents the tracer control element in which ζ , w , S , and T are calculated.

a number of estuaries and coastal oceans that are characterized by highly irregular geometry, large areas of intertidal salt marshes, and steeply sloping bottom topography (see <http://fvcom.smast.umassd.edu> for more information). Validations, in which model predictions are compared with analytical or semianalytical solutions for idealized cases as well as with in situ data for realistic applications, are presented by *Chen et al.* [2003, 2007], *Isobe and Beardsley* [2006], *Weisberg and Zheng* [2006], *Frick et al.* [2007], and *Cowles et al.* [2008]. Previous idealized validation cases include: wind-induced long-surface gravity waves in a circular lake; tidal resonance in rectangular and sector channels; freshwater discharge over the continental shelf with curved coastline; and a thermal bottom boundary layer over the slope with steep bottom topography [*Chen et al.*, 2007]. Comparison between FVCOM and the two structured-grid finite-difference models (the Princeton Ocean Model (POM) and the semi-implicit Estuarine and Coastal Ocean Model (ECOM-si)) illustrates that by employing a better fit to the curvature of the coastline, FVCOM provides improved numerical accuracy and correctly captures the

physics of tide-, wind-, and buoyancy-induced waves and flows in the coastal oceans [*Chen et al.*, 2007].

[5] In addition to the geometric fitting issue, other aspects of the FVCOM numerics need careful validation as well. For example, it is important to examine the sensitivity of the numerical solution to the unstructured mesh topology and the accuracy of FVCOM's nonlinear advection scheme. In view of these validation needs, we address here the following questions: (1) is the FVCOM simulation sensitive to different triangulation methods, and if so, to what degree; (2) does the convergence of the numerical solution depend critically upon the configuration of the unstructured-grid mesh; (3) what are the capabilities of the FVCOM second-order advective flux formulation with and without a discontinuity in the solution; and (4) what is the accuracy of the implicit treatment of the vertical viscosity term? Three new test cases, which are selected from the Regional Ocean Modeling System (ROMS) test suite, are used to evaluate the numerical accuracy of FVCOM. They are the Rossby equatorial soliton case, the hydraulic jump case, and the three-dimensional wind-driven basin case. A model inter-

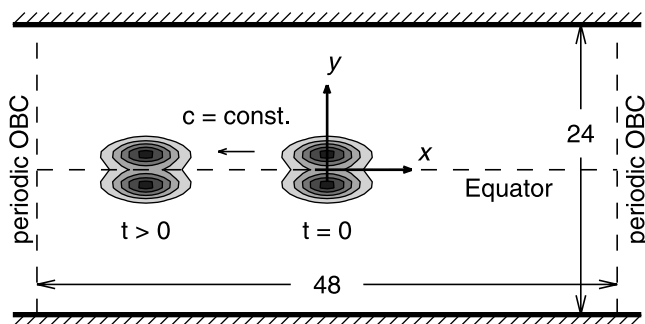


Figure 2. Schematic diagram of the Rossby equatorial soliton test problem. The nondimensional length and width of the channel are 48 and 24, respectively, with periodic open boundary conditions in the east-west direction and no-slip boundary conditions along the north and south boundaries. The analytical solution predicts that the soliton propagates westward at a fixed speed and its shape remains unchanged with time.

comparison is also made to compare the performance of FVCOM with that of ROMS, a popular structured-grid ocean model.

[6] The remainder of this paper is organized as follows. FVCOM and three types of unstructured triangular grids are briefly described in section 2. The results of the three idealized cases are presented in sections 3, 4, and 5, respectively. Conclusions are given in section 6.

2. FVCOM and Unstructured Triangular Grids

[7] FVCOM is a three-dimensional, free-surface, prognostic ocean model consisting of momentum, continuity, temperature, salinity, and density equations. The Boussinesq approximation and hydrostatic assumption are employed in the model. It is closed mathematically using either the Mellor and Yamada level 2.5 [Mellor and Yamada, 1982; Galperin et al., 1988] or the $k-\varepsilon$ [Rodi, 1987; Umlauf and Burchard, 2005] turbulence closure schemes for vertical eddy mixing and the Smagorinsky parameterization for horizontal eddy viscosity and diffusivity [Smagorinsky, 1963]. A σ transformation in the vertical is used to convert irregular bottom topography into a regular computational domain. Time stepping in FVCOM is implemented using a split-explicit approach, in which the free sea surface, defined as the “external mode,” is integrated by solving vertically averaged equations with a smaller time step and the 3-D momentum and tracer equations, defined as the “internal mode,” are integrated with a larger time step. Following every internal time step, an adjustment is made to maintain numerical consistency between the modes [Chen et al., 2006]. A second-order accurate, four-stage Runge-Kutta time stepping scheme is used for external mode time integration and the first-order Euler forward scheme is used for internal mode time integration. A second-order accurate upwind scheme, which is based on piecewise linear reconstruction of dynamic variables, is used for flux calculation of momentum and tracer quantities [Kobayashi et al., 1999; Hubbard, 1999]. A fractional step method is used in the

calculation of three-dimensional (internal) variables, in which the advective and horizontal diffusive fluxes are advanced separately from the vertical diffusive fluxes. The former is explicit whereas the latter is implicit to remove the stability constraint deriving from small vertical spacing.

[8] FVCOM subdivides the horizontal computational domain into a set of nonoverlapping unstructured triangular meshes. An individual triangle is composed of three nodes, a centroid, and three edges (Figure 1a). The horizontal velocity components (u , v) are located at the triangle centroids and the vertical velocity, as well as all scalar variables (temperature, salinity, etc.), are placed at the nodes. The horizontal velocities are computed by net momentum flux across the momentum control element (MCE) bounded by three sides of an individual triangle, while scalar variables at each node are determined by the net flux across the tracer control element (TCE) that is enclosed by lines connecting centroids and middle points of triangle sides in surrounding triangles (Figure 1a).

[9] To test the sensitivity and accuracy of FVCOM simulations, three types of grids are designed in this study with different symmetry properties. In grid A (Figure 1b), triangular nodes and centroids, TCEs, and MCEs are all symmetric relative to the x axis ($y=0$). In grid B (Figure 1c), only node points are distributed symmetrically relative to the x axis. Grid C (Figure 1d) is generated by a commercial grid generation package, SMS8.1 (Surface water Modeling System version 8.1). The triangles in this mesh are generated using a Delaunay-based reconnection of a point insertion scheme and do not exhibit a specific pattern. This last mesh represents a general purpose unstructured grid, normally employed in realistic FVCOM applications.

[10] The horizontal resolution (dx) in FVCOM is defined by the length of an individual triangle edge. In comparison, the horizontal resolution in a structured-grid model, such as ROMS which employs an Arakawa-C grid, is given as the distance between two like variables (e.g., between two temperature points, or between two u points, etc). Hence, for a given rectangular domain and when FVCOM employs a structured triangular grid (such as grid A or grid B in Figure 1), there are more u , v points in FVCOM than in ROMS even though the number of water elevation points are the same for both models. Therefore, FVCOM requires more computational effort than ROMS for a given problem with the same horizontal resolution.

3. Rossby Equatorial Soliton Case

[11] This test problem considers the propagation of a small amplitude Rossby soliton on an equatorial β -plane, which is characterized by a modon with two sea level peaks of equal size and strength decaying exponentially with distance away from their centers. This is a good test case for examining the dispersion and numerical damping of a given model because the shape preservation and constant translation speed of the soliton wave are achieved through a delicate balance between nonlinearity and dispersion.

[12] The model domain consists of a zonal equatorial channel bounded by rigid vertical walls on northern and southern sides and open through a periodic condition in the east-west direction (Figure 2). In nondimensional form, the channel has a length of 48 ($-24 \leq x \leq 24$) and a width of

Table 1. Error Metrics of the FVCOM and ROMS Numerical Solutions for the Rossby Equatorial Soliton Test Case^a

	dx	dt	C_r^+	h_r^+	C_r^-	h_r^-	$\ h\ _2$
Exact solution			1.000	1.000	1.000	1.000	0.0
<i>FVCOM</i>							
Grid A	0.25	0.01	1.001	0.902	1.001	0.902	1.9032×10^{-3}
Grid B	0.25	0.01	0.991	0.850	0.991	0.818	3.5165×10^{-3}
Grid C	0.25	0.01	0.984	0.867	0.985	0.856	3.8614×10^{-3}
Grid A	0.125	0.005	1.001	0.982	1.001	0.982	5.9508×10^{-4}
Grid B	0.125	0.005	0.999	0.967	0.999	0.963	6.0900×10^{-4}
Grid C	0.125	0.005	1.000	0.974	0.999	0.974	5.7450×10^{-4}
Grid A	0.05	0.002	1.000	0.998	1.000	0.998	6.2132×10^{-5}
Grid B	0.05	0.002	1.000	0.996	1.000	0.996	1.0149×10^{-4}
Grid C	0.05	0.002	1.000	0.997	1.000	0.997	5.2339×10^{-5}
Grid C	variable	0.002	1.000	0.997	1.000	0.997	7.2883×10^{-5}
<i>ROMS</i>							
Fourth-order	0.25	0.01	1.011	0.988	1.011	0.988	
Fourth-order	0.125	0.005	1.003	0.996	1.003	0.996	
Fourth-order	0.05	0.002	1.000	0.999	1.000	0.999	

^aFVCOM, Finite-Volume Coastal Ocean Model; ROMS, Regional Ocean Modeling System. Note: dx is the nominal horizontal resolution of the grid (triangle edge length in FVCOM), dt is the time step, $C_r (= (48 - X_{\text{end}})/47.18)$ is the relative mean phase speed of the soliton wave during the 120 time units period, $h_r (= h_{\text{max}}/0.1567020)$ is the relative peak height at time 120, superscript plus sign represents the value for the northern anticyclone, superscript minus sign represents the value for the southern anticyclone, and $\|h\|_2$ is the root-mean-square of the differences between predicted surface height and the “true” solution. The method to find X_{end} and h_{max} is described in section 3. The “true” solution of this problem is obtained by running a high-resolution ($dx = 0.02$) FVCOM numerical experiment. ROMS results are cited from the website of the Ocean Modeling Group (Ocean Modeling Group data are available at <http://marine.rutgers.edu/po/index.php?model=%20test-problems&title=%20soliton&model=test-problems&title=soliton>). The order represents accuracy of the horizontal advection scheme.

24 ($-12 \leq y \leq 12$). Assuming that the water is inviscid, the shallow water equations with a β -plane approximation are given as

$$\frac{\partial Du}{\partial t} + \frac{\partial Du^2}{\partial x} + \frac{\partial Du v}{\partial y} - f Dv = -gD \frac{\partial \zeta}{\partial x} \quad (1)$$

$$\frac{\partial Dv}{\partial t} + \frac{\partial Du v}{\partial x} + \frac{\partial Dv^2}{\partial y} + f Du = -gD \frac{\partial \zeta}{\partial y} \quad (2)$$

$$\frac{\partial \zeta}{\partial t} + \frac{\partial Du}{\partial x} + \frac{\partial Dv}{\partial y} = 0 \quad (3)$$

where u and v are the nondimensional, vertically averaged horizontal velocities in the x - and y -coordinate, $f = f_o + \beta y$ is the Coriolis parameter with $f_o = 0$ and $\beta = 1.0$, ζ is the free surface height relative to the undisturbed sea level, H is the constant water depth of 1.0, $D = H + \zeta$ is the total water column thickness, and g is a nondimensional gravitational constant of 1.0.

[13] The zeroth- and first-order asymptotic solutions of equations (1), (2), and (3), with proper initial and boundary conditions and assumption that the amplitude of the soliton is small, were first derived by Boyd [1980, 1985] and given as

$$u = u^{(o)} + u^{(1)}, \quad v = v^{(o)} + v^{(1)}, \quad \zeta = \zeta^{(o)} + \zeta^{(1)} \quad (4)$$

where the superscripts refer to the order of the asymptotic series and the general form for each term can be found at the ROMS test problem website (<http://marine.rutgers.edu/po/index.php?model=test-problems&title=soliton>).

[14] The initial velocity and sea surface height distributions in numerical experiments are constructed from the zeroth- and first-order asymptotic solutions, with the soliton center initially located at $x = 0$. The two-term perturbation solution shows that the equatorial soliton wave has a constant westward propagation speed $c = c^{(o)} + c^{(1)} = -0.4$ and its double anticyclone structure stays unchanged with time. Hence, the soliton travels over the length of the channel and returns to its initial position in 120 time units because of the periodic conditions at the eastern and western ends. Deviation from shape preservation and uniform propagation speed, however, can arise because of (1) inexact initial condition due to the asymptotic nature of the analytic solution and (2) inexact numerical solutions resulting from approximations used in the finite-volume numerical discretization method. To separate these two errors, a very high resolution FVCOM experiment with the same initial conditions is conducted ($dx = 0.02$, see footnote in Table 1), which shows that the soliton travels 47.18 distance units in 120 time units and its peak height decreases from 0.1672725 at $t = 0$ to 0.1567020 at $t = 120$. The error metrics of numerical experiments are thus constructed by comparing numerical solutions at other resolutions with the result of this experiment. Convergence experiments discussed later suggest that numerical solutions do, indeed, all approach to this high-resolution numerical solution. Thus, the error metrics described below contain mostly the second class of error.

[15] To diagnose the performance of FVCOM, the error metrics are calculated using the same method used in ROMS. First the FVCOM solutions are interpolated onto a reference grid (the $dx = 0.02$ grid in Table 1), assuming that the distribution of surface elevation is piecewise linear in each triangle. Then the maximum surface height value (h_{max}) and its location (X_{end}) at $t = 120$ are determined on

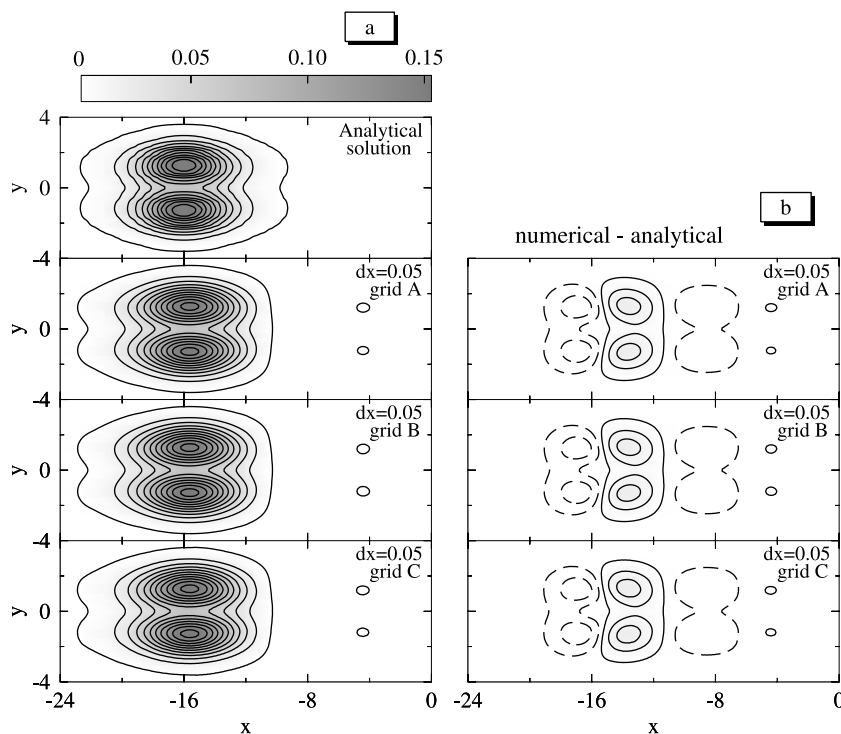


Figure 3. (a) Analytical and FVCOM-predicted sea surface elevation contours at 40 time units for the Rossby soliton test problem. Contour interval is 0.015. (b) Sea surface elevation difference between the analytical solution and the $dx = 0.05$ FVCOM solutions for various grids. Contour interval is 0.0075. Negative contours are dashed.

this reference grid. Finally, the L_2 norm of pointwise error in the surface height field, the relative peak height ($h_r = h_{\max}/0.1567020$), and the relative mean phase speed during the 120 time units period ($C_r = (48 - X_{\text{end}})/47.18$) are calculated from the interpolated field. In this way, the metrics obtained provide a uniform set of diagnostics for proper comparison of the FVCOM- and ROMS-computed results.

[16] The Rossby equatorial soliton consists of two anticyclonic eddies. Hence, for each parameter in the error metrics, there are two values for the northern and southern anticyclones, respectively. The analytic solution is symmetric, indicating that these eddies are of equal strength and size and their centers are equidistant from the equator ($y = 0$). However, numerical solutions obtained using grids that are asymmetric relative to the equator can lead to nonsymmetric solutions. To examine this issue, the three types of grids presented in the last section are all tested. For each grid, numerical experiments are conducted with horizontal resolution (dx) of 0.25, 0.125, and 0.05 respectively. The time step (dt) is scaled accordingly to ensure that the Courant number ($C = c \cdot dt/dx$, where c is the modon propagation speed) remains unchanged. The numerical solution can be considered time step independent at this Courant number.

[17] This test problem is inviscid: the bottom friction and horizontal viscosity are set to zero at all time. FVCOM can be run with zero explicit viscosity.

[18] Metrics for all numerical experiments are summarized in Table 1, where several important aspects of FVCOM performance are highlighted. First, the FVCOM error metrics decrease as the grid is refined. This conver-

gence occurs regardless of the type of grid used. For example, at the lowest spatial resolution ($dx = 0.25$), the maximum surface heights after 120 time units are all below 91% of their initial values, while at $dx = 0.05$ the peak heights approach more than 99% of the theoretical values for all three grids. On the other hand, the soliton celerity is less sensitive to the increase of horizontal resolution. The translation speeds of the northern and southern anticyclones are above 98% of the true values at $dx = 0.25$, and are nearly equal to the speed of the analytical solution when dx is reduced to 0.125.

[19] Second, the symmetric grid (grid A) always gives a solution which is exactly symmetric relative to the equation ($y = 0$), while asymmetric grids (grids B and C) yield solutions that are not symmetric. In addition, the symmetric grid generally yields better results than the asymmetric grids. Nevertheless, the asymmetry caused by asymmetric meshes is reduced as the horizontal resolution is increased. As a result, the difference among the results of experiments with $dx = 0.05$ is negligible (Table 1 and Figure 3). Also evident in Figure 3 is a pair of trailing Kelvin waves that are generated through an adjustment process due to the neglect of higher-order terms in the initial conditions. Similarly, the difference between the northern and southern Kelvin waves diminishes as the grid is refined.

[20] It should be pointed out that the asymmetric solution obtained in FVCOM experiments is related to the asymmetric numerical grid used in the simulation, rather than the numerical algorithm. In any numerical model, whether based on finite-difference, finite-volume, or finite-element methods, if the grid is asymmetrically distributed with

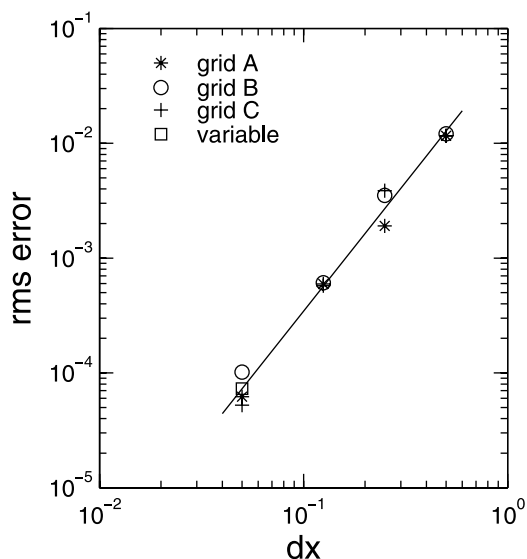


Figure 4. A log-log plot of RMS error of sea surface elevation versus grid size for the Rossby equatorial soliton test problem. The slope of the fitting line, 2.24, shows the FVCOM convergence rate.

respect to the equator, the numerical solution must be asymmetric in a low-resolution case because of the existence of mismatch in the discrete representation of the northern and southern anticyclones.

[21] The FVCOM error convergence rate is given as a function of horizontal resolution in Figure 4, where a log-log plot of root-mean-square (RMS) sea surface elevation error versus grid spacing is shown. The convergence trends for different triangular grids are almost identical. The slope of the fitting line is 2.24, giving the average FVCOM convergence rate. Thus, as implemented, the spatial accuracy of the horizontal advective flux and pressure gradient force in FVCOM is formally second-order. The small disparity may be attributed to the fact that a high-resolution numerical solution, instead of a true analytical solution, is used to calculate the RMS error in surface elevation.

[22] The error metrics of ROMS experiments for the Rossby soliton test problem, with zero explicit viscosity, are cited from the ROMS website and are reproduced in Table 1 using the same numerical ‘true’ solution as used in the analysis of FVCOM. The accuracy of the advection scheme used in ROMS experiments is fourth-order. Since ROMS uses a symmetric grid in its simulations, it yields two identical anticyclones in the northern and southern channel. From Table 1, it can be seen that when the horizontal resolution is coarse (i.e., $dx = 0.25$), the fourth-order advection scheme used in ROMS shows less anticyclone amplitude decay than the second-order advection scheme used in FVCOM. On the contrary, the phase speed of the soliton wave is better simulated by FVCOM with the symmetric grid (grid A). As the horizontal grid size reduces to 0.125, FVCOM and ROMS results are very close in both peak amplitude and wave celerity. When the grid size is reduced to 0.05, FVCOM and ROMS metrics are almost identical, regardless of the type of triangular grid used by FVCOM. The convergence of numerical solutions of dif-

ferent models justifies our practice of using a high-resolution numerical solution as the ‘true’ solution in error metrics calculation.

[23] FVCOM has second-order spatial accuracy, while ROMS has several high-order options in its advection scheme. We believed that second-order is an appropriate compromise between numerical accuracy and computational efficiency for real ocean applications, even though an effort is being made to introduce the high-order Discontinuous Galerkin Method (DGM) [Reed and Hill, 1973] into FVCOM. In the presence of large gradients or fronts, the basic philosophy behind FVCOM model design is to refine the grid resolution in regions of interest and not elsewhere, making use of the flexibility provided by the unstructured triangular grid. As an example, one experiment (Table 1, the FVCOM experiment with variable dx) is conducted in which horizontal grid mesh has a resolution of $dx = 0.05$ in the soliton traverse region and on the order of $dx = 0.5$ outside that region. It can be seen that the error metrics of this experiment are exactly the same as the group of experiments with $dx = 0.05$ uniformly. However, the computation time for the former is only about one third of the latter. The saving in computer time in this case is significant. In general for problems with localized flow phenomena, significant computational saving can be achieved by an efficient distribution of mesh resolution.

4. Hydraulic Jump Case

[24] This test problem consists of supercritical fluid flow through a channel with a constriction. The flow accelerates when it encounters a sudden change in channel cross section, resulting in the formation of a straight-line hydraulic jump emanating from the ramp corner [Alerudo and Garcia-Navarro, 1993; Choi et al., 2004]. It is a good test case for examining the numerical model’s advection scheme in simulating a discontinuous solution.

[25] The model domain is a zonal channel 40 m long and 30 m wide bounded by rigid walls on northern and southern sides and open through an inflow boundary in the west and an outflow boundary in the east (Figure 5). There is a constriction bearing an angle of 8.95° to the horizontal. The water depth H is 1.0 m everywhere. Initially the along-channel velocity component u_0 is chosen to be the same as the inflow value (8.57 m s^{-1}), the cross-channel velocity component v_0 and surface elevation ζ_0 are zero. This corresponds to the Froude number $Fr = |u|/\sqrt{g(H + \zeta)} = 2.74$. At the western open boundary, u , v , ζ are fixed at 8.57 m s^{-1} , 0.0 m s^{-1} , 0.0 m . At the eastern open boundary a zero-gradient condition is employed for the three variables, although no boundary condition is in principle required because the flow is supercritical. At the northern and southern solid boundaries, no-normal flow conditions are used. For this case, the inviscid shallow water equations without Coriolis force (equations (1), (2), and (3)) are employed. The steady state analytical solution downstream of the jump is $\zeta_d = 0.5 \text{ m}$, $u_d = 7.956 \text{ m s}^{-1}$, and $Fr_d = 2.074$; and the angle of the jump is 30° to the east-west direction (Figure 5).

[26] The following metrics of the numerical solution are considered: (1) the minimum ζ value in the domain (indicating undershooting), (2) the maximum ζ value in the

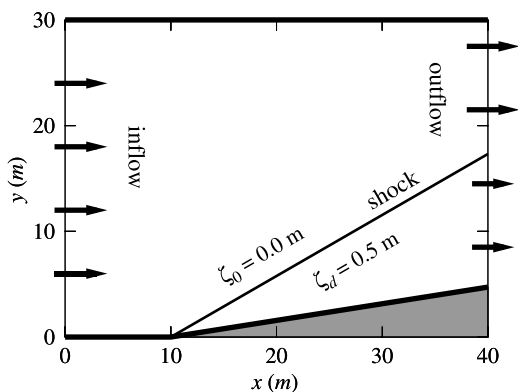


Figure 5. Schematic diagram of the hydraulic jump test problem. The constriction angle between the deflected wall and the x axis is 8.95° ; the shock angle between the shock line and the x axis is 30° .

domain (indicating overshooting), (3) the mean ζ value downstream of the jump, (4) the mean velocity downstream of the jump, (5) the angle of the jump, (6) the mean deviation of the simulated jump from the theoretical line, and (7) the mean thickness of the jump.

[27] These metrics are evaluated in the same way for both FVCOM and ROMS solutions as follows:

[28] 1. For (1) and (2), the global minimum and maximum ζ values are calculated in the computational domain.

[29] 2. For (3) and (4), the mean values are evaluated by first defining a triangular region, 1 m away from the shock, ramp and outer boundary and then taking an area-weighted average of the quantities in this region. Only full grid cells are used in the mean value calculations after checking that their centroids lie within this triangle.

[30] 3. For metrics (5), (6), and (7), 101 cross sections in the y direction are selected that are uniformly distributed between 3 m after the ramp corner and 3 m ahead of the outflow boundary. The x , y locations of $\zeta = 0.25$ m are searched via linear interpolation on each section. A straight-line least squares fit is performed on the x , y values, and (5) is recovered from the line slope. As the exact angle of the jump (30°) is known, the exact y values of the jump on each

section can be evaluated, from which (6) can be extracted. The jump thickness (7) is evaluated by searching for the y coordinates of $\zeta = \zeta_R$ and $\zeta = \zeta_L$ ($\zeta_R = 0.375$ m, $\zeta_L = 0.125$ m) also via linear interpolation and then taking their differences.

[31] The error metrics of FVCOM experiments, using a C-type triangular mesh (Figure 1d), are summarized in Table 2. As can be seen, with no explicit viscosity there are finite-amplitude oscillations in surface elevation field near the hydraulic jump, which cause FVCOM solutions to overshoot ($\zeta_{\max} > 0.5$ m) and undershoot ($\zeta_{\min} < 0$ m). These oscillations can be clearly seen in the cross-section view (Figure 6). An increase in the horizontal resolution does not ameliorate this problem. However, the overshooting and undershooting do not significantly affect the mean elevation or velocity magnitude downstream of the hydraulic jump, as they are very close to the theoretical values regardless of grid refinement. The angle of the discontinuity shows no obvious improvement with grid refinement either. Nevertheless, the mean deviation of the jump position and the jump thickness is greatly improved with increased horizontal resolution (Table 2 and Figure 6).

[32] It is well known that higher than first-order discrete schemes generally produce Gibbs oscillations in regions of unsolved gradients in the solution [LeVeque, 2002]. This is the reason for the appearance of overshooting and undershooting at a discontinuous transition edge in the above experiments. Without special treatment, spurious oscillations exist in finite-difference methods [Haidvogel and Beckmann, 1999], in finite-element methods [Johnson, 1987], as well as in finite-volume methods [LeVeque, 2002]. Two methods are used here to suppress the oscillations near the discontinuity. The first is to introduce explicitly a numerical viscosity. Though FVCOM uses the Smagorinsky horizontal viscosity in default, in order to make the result comparable to ROMS output a constant coefficient harmonic horizontal viscosity is added to the shallow water equations (equations (1), (2), and (3)). Numerical experiments show that the overshooting and undershooting do indeed reduce with the increased viscosity (Table 2). Finite-amplitude oscillations become small amplitude ripples (Figure 7). However, the mean surface

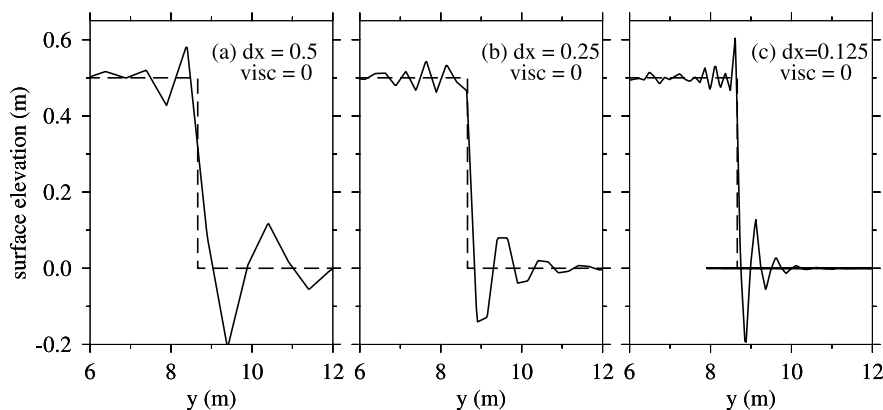


Figure 6. FVCOM calculated sea surface elevation along the section at (solid line) $x = 25$ m in the hydraulic jump test problem. (a) $dx = 0.5$ m, (b) $dx = 0.25$ m, and (c) $dx = 0.125$ m. All three cases are without horizontal viscosity. Dashed line is the analytical solution.

Table 2. Error Metrics of the FVCOM and ROMS Numerical Solutions for the Hydraulic Jump Test Case^a

	dx (m)	dt (s)	ζ_{\min} (m)	ζ_{\max} (m)	$(\zeta_d)_{\text{mean}}$ (m)	$(u_d)_{\text{mean}}$ (m s ⁻¹)	Angle (°)	$ dy $ (m)	Thickness (m)
Exact solution			0	0.5	0.5	7.956	30	0	0
<i>FVCOM</i>									
visc = 0	0.5	0.002	-0.269	0.688	0.500	7.949	29.952	0.111	0.305
visc = 0	0.25	0.001	-0.268	0.697	0.499	7.951	30.030	0.063	0.151
visc = 0	0.125	0.0005	-0.272	0.696	0.500	7.951	30.029	0.037	0.076
visc = 0.6	0.5	0.002	-0.023	0.500	0.497	7.953	29.960	0.106	0.773
visc = 0.3	0.25	0.001	-0.047	0.514	0.508	7.925	30.129	0.129	0.320
visc = 0.15	0.125	0.0005	-0.057	0.515	0.506	7.940	30.093	0.071	0.154
<i>ROMS</i>									
visc = 0.6	0.5	0.002	-0.020	0.497	0.478	7.974	29.331	0.133	0.887
visc = 0.3	0.25	0.001	-0.028	0.512	0.487	7.955	29.339	0.098	0.431
visc = 0.15	0.15	0.0005	-0.050	0.541	0.491	7.945	29.364	0.125	0.213

^aNote: dx is the nominal horizontal resolution of the grid (triangle edge length in FVCOM), dt is the time step; ζ_{\min} and ζ_{\max} are the minimum and maximum surface elevation in the domain, $(\zeta_d)_{\text{mean}}$ and $(u_d)_{\text{mean}}$ are the mean surface elevation and mean velocity downstream of the jump, Angle is the angle of the jump, $|dy|$ is the mean deviation of the simulated jump from the theoretical line, and Thickness is the mean thickness of the jump. The method to calculate $(\zeta_d)_{\text{mean}}$, $(u_d)_{\text{mean}}$, Angle, $|dy|$, and Thickness is described in section 4. ROMS results are cited from the Rutgers IMCS Ocean Modeling Group (Rutgers IMCS Ocean Modeling Group data are available at <http://marine.rutgers.edu/po/index.php?model=test-problems&title=supercritical>). The parameter visc is the harmonic horizontal viscosity coefficient used in both FVCOM and ROMS experiments.

elevation and mean velocity downstream of the jump are somewhat sensitive to the value of viscosity coefficient used and deviate from the exact solution. The shock angle and the mean deviation of the jump position are almost unaffected comparing to the zero viscosity case. The most conspicuous change is in jump thickness, which nearly doubles with the increase in viscosity (Table 2).

[33] The second method used in FVCOM, which is able to capture shocks without introducing explicit viscosity, is called multidimensional slope limiting [Barth and Jespersen, 1989; Hubbard, 1999]. First-order upwind methods are known to be monotone and resolve discontinuities without producing any oscillations. However, in smooth portions of the flow, first-order accuracy is generally not sufficient. Second-order methods such as those used in FVCOM give better accuracy in smooth flow, but produce oscillations in the vicinity of discontinuities. Multidimensional slope limiters are designed to be second-order accurate in smooth portions of the flow and reduce to a first-order upwind scheme near discontinuities. In this manner, higher-order monotone methods are constructed. Applying the slope limiter described by Hubbard [1999] to FVCOM, numerical experiments show that the overshooting and undershooting are completely suppressed near the discontinuity (Figure 8). In addition, slope limiter method yields similar accuracy on mean elevation and velocity after the jump, the jump angle, and the jump location when comparing with the cases with horizontal viscosity. The main difference lies in the jump thickness, which is thicker in the former case. For example, when $dx = 0.5$ m the jump is 0.773 m thick for a horizontal viscosity coefficient of 0.6 while it is 0.888 m for the slope limiter experiment; the thickness is 0.154 m and 0.226 m, respectively, when $dx = 0.125$ m.

[34] ROMS numerical experiments for this test problem as given in the ROMS website are reproduced in Table 2. All of the ROMS numerical computations listed on that website require numerical viscosity without which the steady state cannot be achieved (long-period oscillations persist in the volume-averaged kinetic and potential energies). This is different from the FVCOM experiments, in

which a steady state can be reached without any explicit horizontal viscosity (Figure 9).

[35] With the inclusion of a constant coefficient harmonic horizontal viscosity, ROMS-computed results also display overshooting and undershooting that are on the same order as FVCOM results computed with the same viscosity. For some other error metrics, ROMS experiments show relatively larger errors than the corresponding FVCOM experiments. For example, the area-mean elevation after the jump: theoretical value is 0.5 m; in the FVCOM results, the values lies between 0.497 m and 0.508 m; and in ROMS between 0.478 m and 0.491 m. For the jump angle: the theoretical value is 30°; in FVCOM results the value lies between 29.960° and 30.129°; and in ROMS ranges from 29.331° to 29.364°.

[36] In this hydraulic jump test case, FVCOM shows better agreements to the analytical solution than ROMS does. The difference results mainly from the employment of slope limiters in the FVCOM flux formulation. When the test cases were completed with ROMS, slope limiters (or

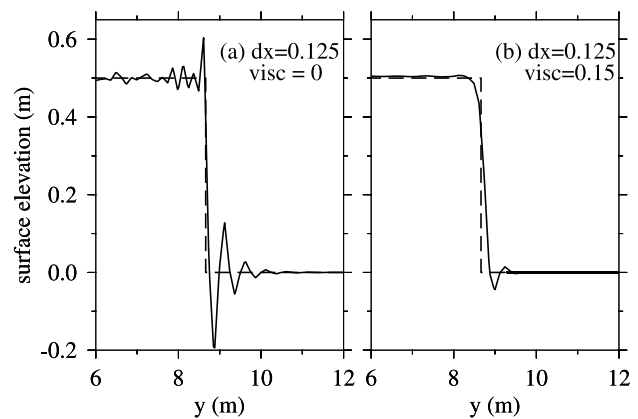


Figure 7. FVCOM calculated sea surface elevation along the section at (solid line) $x = 25$ m in the hydraulic jump test problem (a) without horizontal viscosity and (b) with horizontal viscosity. Dashed line is the analytical solution.

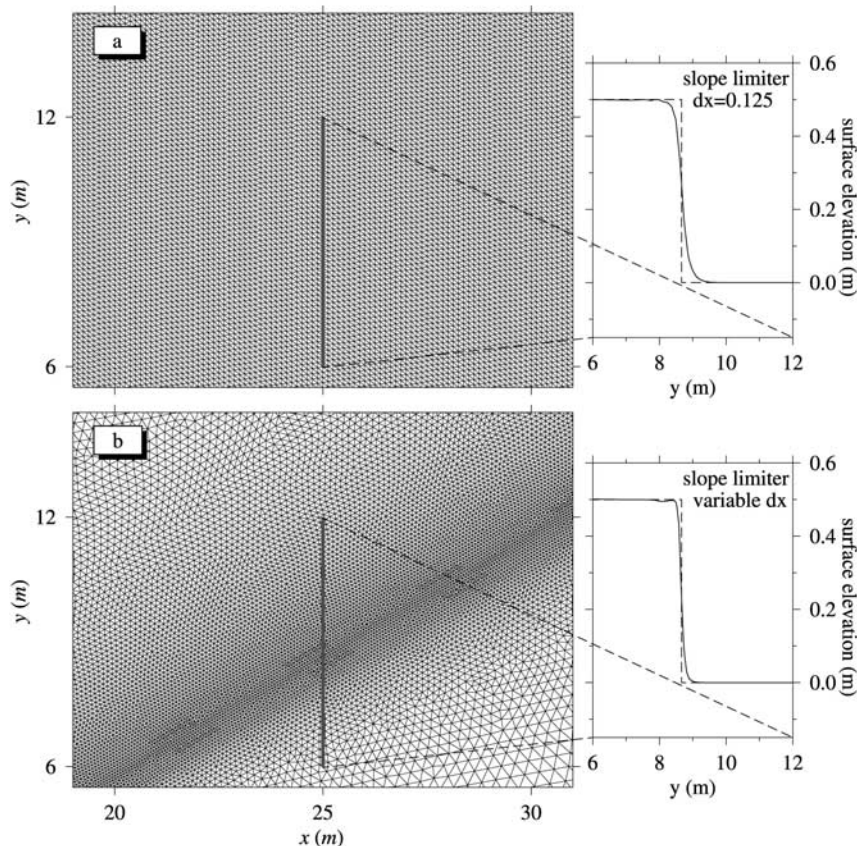


Figure 8. FVCOM calculated sea surface elevation with (a) uniform grid size ($dx = 0.125$ m) and (b) variable grid size ($dx = 0.075$ m near shock and $dx = 0.5$ m away from shock) in the hydraulic jump test problem. A slope limiter is used in the calculation.

flux limiters) were not available in the coding, although with some effort they could be implemented. In addition, ROMS is no longer a finite-volume model when curvilinear grid is used in this test case because of the inclusion of curvature terms and the approximation used in the calculation of area of its control volume. Finite-volume methods are able to naturally resolve the jump conditions across a discontinuity exactly when applied to the solution of hyperbolic conservation laws [LeVeque, 1990]. It is for this reason that development of finite-volume methods has been closely associated with computational fluid dynamics applications involving sharp discontinuities and shocks. In geophysical fluid dynamics problems, true discontinuities are not normally present, but strong fronts can evolve, and their accurate solution is a concern. This case illustrates that FVCOM has some advantages in this regard.

[37] To further illustrate the local refinement capacity of FVCOM, an experiment with variable grid size is designed in which the triangle sides are on the order of 0.075 m along the shock line and gradually increase to 0.5 m away from the shock (Figure 8b). A slope limiter is used in the calculation. In this experiment the simulated jump thickness is less than half of that in the experiment with uniformly $dx = 0.125$ m (Figure 8a). Using the variable grid size, this experiment increases the numerical simulation accuracy while decreasing the total number of triangular cells in the

domain. Thus, the computation time is reduced by more than half.

[38] One caveat concerning the present FVCOM-ROMS comparison is that the results represent the capabilities of the solvers at one point in time. Both models have active model teams and are thus in constant state of improvement. Since the completion of the present validation experiments, a third-order upwind scheme has been added to ROMS as a spatial flux discretization. This scheme is quasi-monotonic and weakly dissipative and the performance of the operator greatly exceeds that of the second- or fourth-order operators used in this paper [Haidvogel *et al.*, 2008]. However, at the current time, no updated results for these test cases are available.

5. Three-Dimensional Wind-Driven Basin Case

[39] This test problem describes a three-dimensional, linear, homogeneous, wind-driven flow in a rotating basin [Winant, 2004]. It is a rare case in which an analytical solution exists for a three-dimensional basin flow and is used here to verify the accuracy of FVCOM's implicit vertical viscosity scheme. Considering a rectangular closed basin with length $2L$ ($-L \leq x \leq L$) and width $2B$ ($-B \leq y \leq B$) on an f plane (Figure 10), the three-dimensional linearized governing equations for the steady flow are

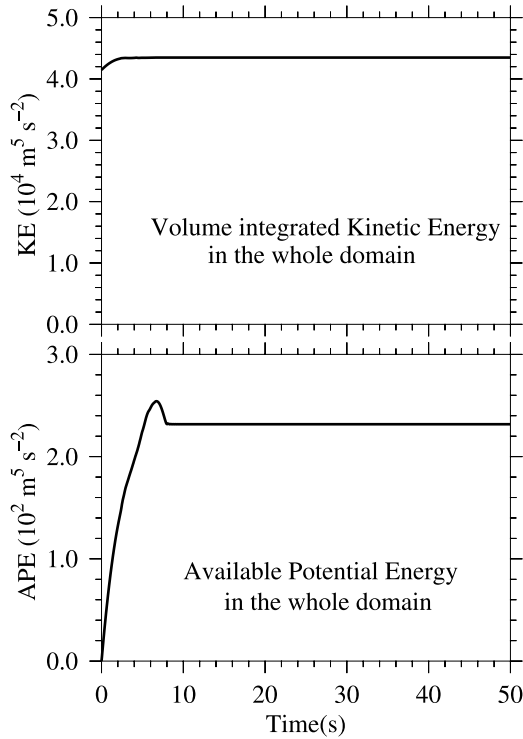


Figure 9. Time series of volume integrated kinetic energy and available potential energy in FVCOM experiment of $dx = 0.125$ m and no explicit viscosity.

$$\nabla \cdot \vec{v} + w_z = 0 \quad (5)$$

$$f\vec{k} \times \vec{v} = -g\nabla\eta + K_m \frac{\partial^2 \vec{v}}{\partial z^2} \quad (6)$$

where $\vec{v}(x, y, z)$ is the horizontal velocity vector and other variables are conventional. The boundary conditions are specified as

$$\vec{v}_z = \frac{\vec{\tau}_s}{\rho K_m} \text{ and } w = 0, \text{ at } z = 0 \quad (7)$$

$$\vec{v} = 0 \text{ and } w = 0, \text{ at } z = -h \quad (8)$$

$$U_n = 0, \text{ at } x = \pm L \text{ and } y = \pm B \quad (9)$$

where $\vec{\tau}_s$ is the surface wind stress and U_n is the vertically averaged volume transport normal to the solid lateral boundaries.

[40] Equations (5) and (6) can be solved analytically [Winant, 2004]. The solution procedure consists of two steps. In the first step, the three-dimensional structure of the horizontal velocities (u, v) are obtained as a function of sea surface elevation gradients by solving the Ekman equations (6) with boundary conditions (7) and (8). To obtain the surface elevation field in the second step, the

vertically averaged momentum equations and continuity equation are used to derive the controlling equation for the transport stream function (equation (23) in Winant, 2004). To solve this equation, one only needs to impose the condition that the transport across lateral boundaries is zero (equation (9)).

[41] The bathymetry of this problem is given by

$$h = h_0 \left\{ 0.08 + 0.92 * \left[X(x/L) \left(1 - (y/B)^2 \right) \right] \right\}, \quad -L \leq x \leq L, -B \leq y \leq B \quad (10)$$

where $X(x)$ is a function of the form

$$X(x) = \begin{cases} 1, & |x| < 1 - \Delta x \\ 1 - \left[\frac{|x| - 1 + \Delta x}{\Delta x} \right]^2, & |x| \geq 1 - \Delta x \end{cases} \quad (11)$$

and Δx is a constant specified as 0.3% of the total length of the basin.

[42] In all numerical experiments, the basin is 200 km long and 50 km wide (i.e., $L = 100$ km and $B = 25$ km). The Coriolis parameter is taken as a constant value of $f = 10^{-4} \text{ s}^{-1}$. The vertical eddy viscosity is set to the constant $K_m = 4 \times 10^{-3} \text{ m}^2 \text{ s}^{-1}$. The maximum water depth $h_0 = 50$ m. The wind stress is specified in the x -direction and wind forcing is linearly ramped up to a constant value of $\tau_x = 0.1$ Pa over a 2 day period.

[43] The analytical solution is derived on the basis of the no-slip bottom boundary condition (equation (8)), whereas there is no corresponding condition in FVCOM and ROMS. The bottom boundary condition commonly used in ocean models usually assumes that the bottom stress is proportional to the near-bottom velocity or velocity squared. In order to make both model simulations conform closely to the no-slip condition, the bottom stress is parameterized as

$$\vec{\tau}_b = \rho K_m \frac{\partial \vec{u}}{\partial z} \approx \rho K_m \frac{\vec{u}_{KB} - 0}{\Delta h} = \rho K_m \frac{\vec{u}_{KB}}{\Delta h} \quad (12)$$

where \vec{u}_{KB} is the velocity vector at the lowest model level and Δh is the distance between the lowest model level and the ocean bottom. Thus, the linear friction coefficient can be

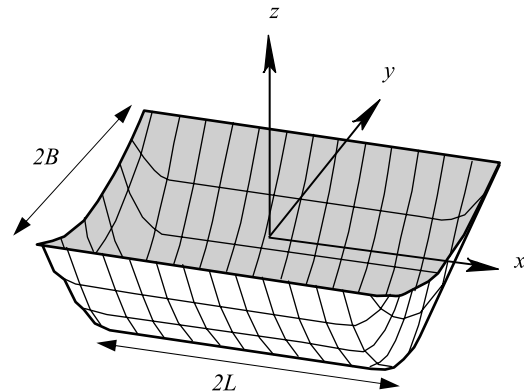


Figure 10. Schematic diagram of the three-dimensional wind-driven basin test problem.

Table 3. Error Metrics of the FVCOM and ROMS Numerical Solutions for the Three-Dimensional Wind-Driven Basin Case^a

dx (km)	dy (km)	σ	$\ \Psi\ _2$ ($10^3 \text{ m}^2 \text{ s}^{-1}$)	$\ u\ _\infty$ (cm s^{-1})	$\ v\ _\infty$ (cm s^{-1})	$\ w\ _\infty$ ($10^{-3} \text{ cm s}^{-1}$)	$\ u\ _2$ (cm s^{-1})	$\ v\ _2$ (cm s^{-1})	$\ w\ _2$ ($10^{-3} \text{ cm s}^{-1}$)	Σ (cm s^{-1})
<i>FVCOM</i>										
Grid A										
4	2	25	0.403	0.395	0.343	1.603	0.127	0.146	0.466	0.274
2	1	25	0.171	0.164	0.195	0.468	0.068	0.076	0.130	0.144
1	0.5	25	0.122	0.135	0.100	0.251	0.054	0.040	0.063	0.095
<i>ROMS</i>										
4	2	25	0.598	0.955	0.527	1.231	0.271	0.166	0.297	0.438
2	1	25	0.567	1.051	0.401	0.759	0.305	0.136	0.201	0.441
1	0.5	25	0.694	1.080	0.400	0.660	0.314	0.129	0.182	0.443

^aTwenty-five sigma layers are used for all runs. Note: dx and dy are the horizontal resolutions of the grid in the x - and y -coordinate, respectively (triangle edge length in FVCOM); σ is the number of sigma layer in the vertical; $\|\Psi\|_2$ is the root-mean-square of the differences between predicted transport stream function and the analytical solution; $\|u\|_\infty$, $\|v\|_\infty$, and $\|w\|_\infty$ are the L_∞ norm of u , v , and w error on the midbasin cross section, respectively; $\|u\|_2$, $\|v\|_2$, and $\|w\|_2$ are the L_2 norm (i.e., root-mean-square) of u , v , and w error on the midbasin cross section, respectively; $\Sigma = \|u\|_2 + \|v\|_2 + \|w\|_2$.

defined as $K_m/\Delta h$. Another method, which recovers the no-slip condition from a linear drag law, is to define the drag coefficient to be a very large number (M. Iskandarani et al., The importance of being viscous; or, how the hydrostatic primitive equations enforce lateral boundary conditions, submitted to *Ocean Modeling*, 2008). However, this method makes \bar{u}_{KB} approach zero instead of the velocity at the ocean bottom. Therefore, the deviation from the analytical solution is larger in the latter case than in the former. The results reported below are all from numerical experiment runs with condition (12).

[44] Performance of the FVCOM and ROMS models is evaluated by comparing to the following characteristics of the analytical solution: (1) the horizontal structure of the transport stream function, and (2) the vertical cross sections of u , v , and w in the middle of the basin ($x = 0$). To explore the sensitivity of FVCOM simulations to different unstructured meshes, two kinds of grids are used in the calculations (grid A and B in Figure 1). ROMS results are computed on a regular rectangular grid. Numerical experiments for both models show that the model solution approaches a steady state in less than 10 simulation days. Hence, the model output at day 10 is used to compare with the analytical solution.

[45] Tables 3 and 4 summarize the FVCOM and ROMS error metrics for various experiments. The FVCOM solutions are obtained using a symmetric grid (grid A). One interesting feature worth noting is that for FVCOM the L_2 norm of the transport stream function error decreases when

the horizontal resolution is increased and vertical resolution is fixed (Table 3) while this error is less sensitive to the change in vertical resolution (Table 4). On the contrary, the same error for ROMS experiments is more sensitive to the reduction in vertical spacing (Table 4) and it does not decrease at all when only horizontal resolution is increased (Table 3). A similar trend can also be found in the L_2 and L_∞ norms of the u , v , w errors in the midbasin section, as well as in FVCOM runs employing the asymmetric grid (grid B).

[46] The stream functions for analytical and numerical solutions computed using 25 sigma layers are illustrated in Figure 11. It can be seen that the structure of the northern and southern gyres is symmetric for both ROMS and FVCOM (with symmetric grid). The narrow regions corresponding to the Stommel boundary layers and the broad turning areas corresponding to the Sverdrup boundary layers [Winant, 2004] are qualitatively well reproduced in both models. The major difference lies in the predicted maximum and minimum stream function values. The FVCOM result is closer to the analytical solution than the ROMS result. Similar conclusion can be drawn from the comparison of model predicted u , v , and w distributions in the midbasin cross section (Figure 12 and Table 3). However, it should be pointed out that the difference between FVCOM and ROMS results is not significant considering the fact that, for example, the magnitude of u velocity in the midbasin section is on the order of 20 cm s^{-1} and the

Table 4. Error Metrics of the FVCOM and ROMS Numerical Solutions for the Three-Dimensional Wind-Driven Basin Case, in Which the Horizontal Resolution is Fixed^a

dx (km)	dy (km)	σ	$\ \Psi\ _2$ ($10^3 \text{ m}^2 \text{ s}^{-1}$)	$\ u\ _\infty$ (cm s^{-1})	$\ v\ _\infty$ (cm s^{-1})	$\ w\ _\infty$ ($10^{-3} \text{ cm s}^{-1}$)	$\ u\ _2$ (cm s^{-1})	$\ v\ _2$ (cm s^{-1})	$\ w\ _2$ ($10^{-3} \text{ cm s}^{-1}$)	Σ (cm s^{-1})
<i>FVCOM</i>										
Grid A										
2	1	13	0.280	0.320	0.216	0.863	0.139	0.085	0.184	0.224
2	1	25	0.171	0.164	0.195	0.468	0.068	0.076	0.130	0.144
2	1	50	0.156	0.161	0.197	0.473	0.054	0.075	0.128	0.129
<i>ROMS</i>										
2	1	13	0.808	1.421	0.735	0.968	0.483	0.217	0.248	0.700
2	1	25	0.567	1.051	0.401	0.759	0.305	0.136	0.201	0.441
2	1	50	0.477	0.850	0.273	0.616	0.234	0.109	0.172	0.343

^aVariable definitions are the same as in Table 3.

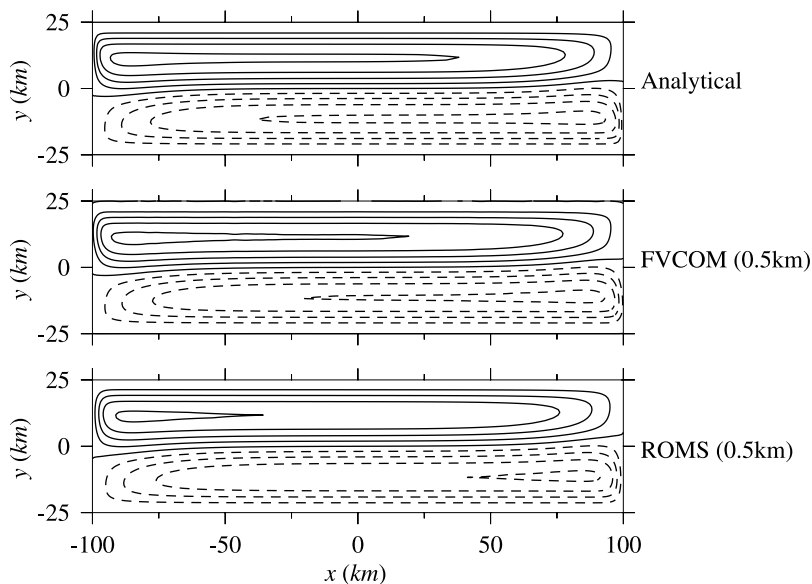


Figure 11. Comparison of the transport stream function for the analytical, FVCOM (using grid A) and ROMS solutions. For both the FVCOM and ROMS experiments, 25 vertical sigma layers are used. The contour interval is $0.005 \times 10^6 \text{ m}^3 \text{ s}^{-1}$. Solid lines represent positive values, while dashed lines represent negative values.

maximum value in u error ($\|u\|_{\infty}$) is on the order of 1 cm s^{-1} for ROMS and 0.4 cm s^{-1} for FVCOM.

[47] In this simple test case, the symmetric grid (grid A) generally yields better results than the asymmetric grid (grid B). When the asymmetric grid is used, FVCOM experiments show that the structure of the northern and southern gyres is not symmetric. As we pointed out in the Rossby soliton test case, when the horizontal resolution is low, no matter what type of numerical model is used, the numerical solution will depend on the grid distribution. The evaluation of the accuracy of a model should be to test if the numerical solution with an arbitrary grid will converge to the true solution as the horizontal resolution is increased. This convergence capability is demonstrated by FVCOM, in which the asymmetry in the numerical solution in the grid B case is gradually reduced and the model stream function converges to the analytical solution as the horizontal resolution is increased.

[48] The convergence rate estimated from the sum of RMS errors of three velocity components (\sum in Table 3) is approximately 0.84 for FVCOM experiments (Figure 13). Even if we increase the horizontal and vertical resolutions simultaneously, the corresponding convergence rate is still significantly less than two (~ 1.14). The spatial accuracy of the FVCOM external mode calculation is second-order, which has been confirmed by the first test problem. By design, the internal mode of FVCOM is also second-order accurate. The less than second-order spatial accuracy demonstrated by this test case is probably related to the approximation in the treatment of the no-slip bottom boundary condition. The numerical convergence rate for ROMS experiments is also less than one, probably because of the same reason.

[49] In this linear barotropic test problem, only the numerics of the vertical eddy viscosity, the Coriolis force,

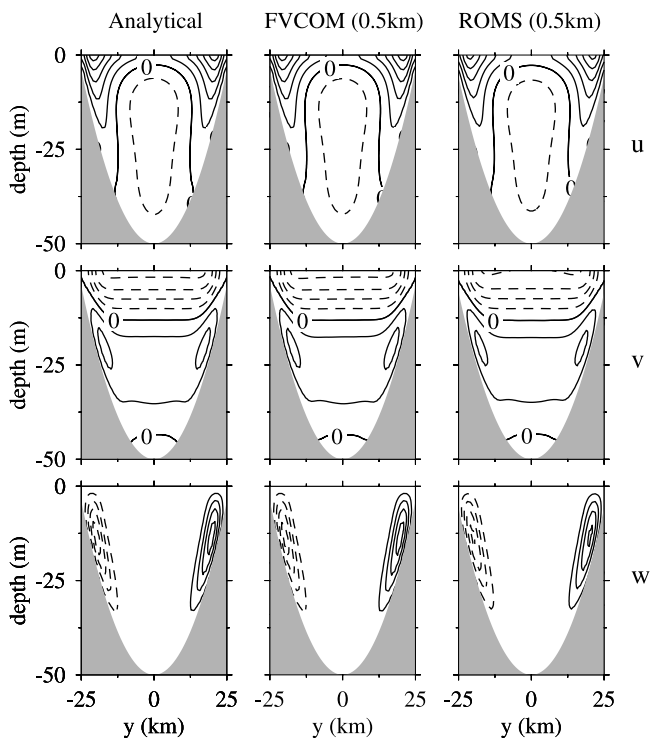


Figure 12. Comparison of u , v , and w distributions at the midbasin section ($x = 0$) for the analytical, FVCOM (using grid A), and ROMS solutions. For both the FVCOM and ROMS experiments, 25 vertical sigma layers are used. Contour intervals are 5 , 2 , and $3 \times 10^{-3} \text{ cm s}^{-1}$ for u , v , and w , respectively. Solid lines represent positive values, while dashed lines represent negative values.

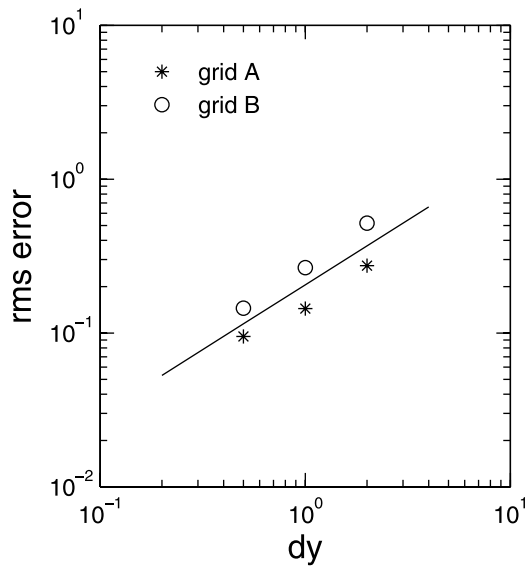


Figure 13. A log-log plot of RMS error of the sum of three velocity components versus grid size for the three-dimensional wind-driven basin test problem. In these FVCOM experiments, the number of sigma layers is kept at 25. The slope of the fitting line is 0.84.

the barotropic pressure gradient force, the continuity equation, and the adjustment between the internal and external mode are included. FVCOM and ROMS both use implicit schemes similar to that used in POM for the computation of vertical viscosity. The treatment of the Coriolis force and the continuity equation are also analogous. Therefore, we suspect that the difference in model sensitivity to the horizontal and vertical resolution is probably related to the numerical treatment of the barotropic pressure gradient term and the adjustment between the internal and external modes. Although the cause of this issue deserves further investigation, the finding from this test case should be instrumental in the design and interpretation of real world applications.

[50] M. Iskandarani et al. (submitted manuscript, 2008) pointed out the role played by the horizontal viscous term in the specification of lateral solid boundary conditions, and attributes the success of ROMS in simulating this horizontally inviscid, wind-driven basin case to its ability being “able to tolerate one-grid-point lateral boundary layers.” We agree with them in that in order to get a physically meaningful solution, additional term(s) omitted in the scale analysis, such as the horizontal viscosity, need to be included in order to satisfy the no normal flow boundary condition. However, we do not think that the success of ROMS in this problem is due to artificial numerical viscosity as they suggest. For this linear problem, the analytical solution can be derived under a condition of zero vertically integrated transport normal to the wall, with no need to enforce the zero normal current at the wall. FVCOM and ROMS are solved similarly by the split-mode approach, which automatically satisfies the zero vertically integrated transport normal to the wall in the external mode. Because of neglect of horizontal advection and viscosity, the zero normal flow condition is not enforced in the calculation of

the 3-D velocity (i.e., the internal mode). This is the reason why these two models can reproduce the analytical solutions derived by Winant [2004].

6. Conclusion

[51] Comparison between the FVCOM-computed and the analytical solutions for the three barotropic test cases demonstrate that the unstructured-grid finite-volume method used in FVCOM provides an overall second-order spatial accuracy for the vertically averaged momentum equations and the continuity equation (i.e., external mode). This model shows the same convergence rate toward the analytical solutions with the increase of the horizontal resolution regardless of the type of triangular grids.

[52] Comparison between the FVCOM and ROMS solutions illustrates that for linear problems in simple idealized domains, the accuracy of the two models is similar. In a highly nonlinear case such as the Rossby equatorial soliton, the second-order advection scheme used in FVCOM is almost as accurate as the fourth-order advection scheme used in ROMS if the horizontal resolution is relatively high. Nevertheless, the current version of FVCOM has its advantage over the current version of ROMS in dealing with discontinuities or large gradients in the solution. Many new numerical techniques in the field of computational fluid dynamics can be used in FVCOM to further improve its performance in this regard.

[53] The three-dimensional wind-driven basin case shows that FVCOM and ROMS simulations have quite a different response to the refinement of grid size in the horizontal and in the vertical. This finding should be taken into account in model selection and the design of horizontal/vertical resolution for realistic applications.

[54] All three test cases discussed in this study encompass rectangular or polygonal domains. In general, the flexibility of the unstructured triangular grid in approximating complex coastal geometry makes FVCOM more suitable to apply in coastal regions and estuaries characterized by irregular coastal geometry. This has been demonstrated in previous FVCOM validation experiments through comparisons with POM and ECOM-si [Chen et al., 2007]. In this study, it is demonstrated that the ability of FVCOM to easily make local grid refinement allows FVCOM to subsequently achieve higher numerical accuracy and, at the same time, higher computational efficiency. These merits are what the structured-grid ocean models lack and what we believe represent the future of coastal/estuarine modeling.

[55] **Acknowledgments.** For this work, H. Huang and G. Cowles were supported by the Massachusetts Marine Fisheries Institute (MFI) through NOAA grants DOC/NOAA/NA04NMF4720332 and DOC/NOAA/NA05NMF472113; C. Chen was supported by NSF grants (OCE0234545, OCE0606928, OCE0712903, OCE0732084, and OCE0726851), NOAA grants (NA160P2323, NA06RG0029, and NA960P0113), MIT Sea grant (2006-RC-103), and Georgia Sea grant (NA26RG0373 and NA66RG0282); C. Winant was supported through NSF grant OCE-0726673; R. Beardsley was supported through NSF OCE-0227679 and the WHOI Smith Chair; K. Hedstrom was supported through NASA grant NAG13-03021 and the Arctic Region Supercomputing Center; and D. Haidvogel was supported through grants ONR N00014-03-1-0683 and NSF OCE 043557. We thank B. Rothschild and K. Stokesbury, leaders of the MFI, for their support of the FVCOM development effort. We also appreciate help from scientists, postdoctoral researchers, and

graduate students in the Marine Ecosystem Dynamic Laboratory, School for Marine Science and Technology, UMASSD, who have contributed to the updating and bug cleaning of the FVCOM code used in this study.

References

- Alcrudo, F., and P. Garcia-Navarro (1993), A high-resolution Godunov-type scheme in finite volumes for the 2D shallow-water equations, *Int. J. Numer. Methods Fluids*, *16*, 489–505, doi:10.1002/flid.1650160604.
- Barth, T. J., and D. C. Jespersen (1989), The design and application of upwind schemes on unstructured meshes, *ALAA Pap.*, *89-0366*, 1–12.
- Boyd, J. P. (1980), Equatorial solitary waves. Part 1: Rossby solitons, *J. Phys. Oceanogr.*, *10*, 1699–1717, doi:10.1175/1520-0485(1980)010<1699:ESWPIR>2.0.CO;2.
- Boyd, J. P. (1985), Equatorial solitary waves. Part 3: Westward-traveling modons, *J. Phys. Oceanogr.*, *15*, 46–54, doi:10.1175/1520-0485(1985)015<0046:ESWPWT>2.0.CO;2.
- Chen, C., H. Liu, and R. C. Beardsley (2003), An unstructured grid, finite-volume, three-dimensional, primitive equations ocean model: Application to coastal ocean and estuaries, *J. Atmos. Oceanic Technol.*, *20*, 159–186, doi:10.1175/1520-0426(2003)020<0159:AUGFVT>2.0.CO;2.
- Chen, C., R. C. Beardsley, and G. Cowles (2006), An unstructured grid, finite-volume coastal ocean model: FVCOM user manual, manual, 315 pp., Sch. for Mar. Sci. and Technol., Univ. of Mass. Dartmouth, New Bedford, Mass.
- Chen, C., H. Huang, R. C. Beardsley, H. Liu, Q. Xu, and G. Cowles (2007), A finite-volume numerical approach for coastal ocean circulation studies: Comparisons with finite difference models, *J. Geophys. Res.*, *112*, C03018, doi:10.1029/2006JC003485.
- Cheng, R. T., and V. Casulli (2003), Modeling a three-dimensional river plume over continental shelf using a 3D unstructured grid model, paper presented at 8th International Conference, Am. Soc. of Civ. Eng., Monterey, Calif., 3–5 Nov.
- Choi, B., M. Iskandarani, J. Levin, and D. B. Haidvogel (2004), A spectral finite-volume method for the shallow water equations, *Mon. Weather Rev.*, *132*, 1777–1791, doi:10.1175/1520-0493(2004)132<1777:ASFMT>2.0.CO;2.
- Cowles, G. W. (2008), Parallelization of the FVCOM coastal ocean model, *Int. J. High Performance Comput. Appl.*, *22*(2), 177–193, doi:10.1177/1094342007083804.
- Cowles, G. W., S. J. Lentz, C. Chen, Q. Xu, and R. C. Beardsley (2008), Comparison of observed and model-computed low frequency circulation and hydrography on the New England Shelf, *J. Geophys. Res.*, doi:10.1029/2007JC004394, in press.
- Frick, W. E., T. Khangaonkar, A. C. Sigleo, and Z. Yang (2007), Estuarine-ocean exchange in a North Pacific estuary: Comparison of steady state and dynamic models, *Estuarine Coastal Shelf Sci.*, *74*(1–2), 1–11, doi:10.1016/j.ecss.2007.02.019.
- Galperin, B., L. H. Kantha, S. Hassid, and A. Rosati (1988), A quasi-equilibrium turbulent energy model for geophysical flows, *J. Atmos. Sci.*, *45*, 55–62, doi:10.1175/1520-0469(1988)045<0055:AQE-TEM>2.0.CO;2.
- Haidvogel, D. B., and A. Beckmann (1999), *Numerical Ocean Circulation Modeling*, 318 pp., Imp. Coll. Press, London.
- Haidvogel, D. B., et al. (2008), Ocean forecasting in terrain-following coordinates: Formulation and skill assessment of the regional ocean modeling system, *J. Comput. Phys.*, *227*, 3595–3624.
- Hubbard, M. E. (1999), Multidimensional slope limiters for MUSCL-type finite volume schemes on unstructured grids, *J. Comput. Phys.*, *155*, 54–74, doi:10.1006/jcph.1999.6329.
- Isobe, A., and R. C. Beardsley (2006), An estimate of the cross-frontal transport at the shelf break of the East China Sea with the finite volume coastal ocean model, *J. Geophys. Res.*, *111*, C03012, doi:10.1029/2005JC003290.
- Johnson, C. (1987), *Numerical Solution of Partial Differential Equations by the Finite Element Method*, 276 pp., Cambridge Univ. Press, New York.
- Kobayashi, M. H., J. M. C. Pereira, and J. C. F. Pereira (1999), A conservative finite-volume second-order-accurate projection method on hybrid unstructured grids, *J. Comput. Phys.*, *150*, 40–75, doi:10.1006/jcph.1998.6163.
- LeVeque, R. J. (1990), *Numerical Methods for Conservation Laws: Lectures in Mathematics*, Eidgenossische Tech. Hochsch., Zurich, Basel, Switzerland.
- LeVeque, R. J. (2002), *Finite Volume Methods for Hyperbolic Problems*, 558 pp., Cambridge Univ. Press, New York.
- Marshall, J., A. Adcroft, C. Hill, L. Perelman, and C. Heisey (1997), A finite-volume, incompressible Navier-Stokes model for studies of the ocean on parallel computers, *J. Geophys. Res.*, *102*, 5753–5766, doi:10.1029/96JC02775.
- Mellor, G. L., and T. Yamada (1982), Development of a turbulence closure model for geophysical fluid problem, *Rev. Geophys.*, *20*, 851–875, doi:10.1029/RG020i004p00851.
- Reed, W. H., and T. R. Hill (1973), Triangular mesh methods for the neutron transport equation, *Tech. Rep. LA-UR-73-479*, Los Alamos Sci. Lab., Los Alamos, N. M.
- Rodi, W. (1987), Examples of calculation methods for flow and mixing in stratified fluid, *J. Geophys. Res.*, *92*, 5305–5328, doi:10.1029/JC092iC05p05305.
- Smagorinsky, J. (1963), General circulation experiments with the primitive equations. I. The basic experiment, *Mon. Weather Rev.*, *91*, 99–164, doi:10.1175/1520-0493(1963)091<0099:GCEWTP>2.3.CO;2.
- Umlauf, L., and H. Burchard (2005), Second-order turbulence closure models for geophysical boundary layers: A review of recent work, *Cont. Shelf Res.*, *25*, 795–827, doi:10.1016/j.csr.2004.08.004.
- Ward, M. C. (1999), An unsteady finite volume circulation model, paper presented at 6th International Conference, Am. Soc. of Civ. Eng., New Orleans, La., 3–5 Nov.
- Weisberg, R. H., and L. Y. Zheng (2006), Circulation of Tampa Bay driven by buoyancy, tides, and winds, as simulated using a finite volume coastal ocean model, *J. Geophys. Res.*, *111*, C01005, doi:10.1029/2005JC003067.
- Winant, C. D. (2004), Three-dimensional wind-driven flow in an elongated, rotating basin, *J. Phys. Oceanogr.*, *34*, 462–476, doi:10.1175/1520-0485(2004)034<0462:TWFIAE>2.0.CO;2.

R. C. Beardsley, Department of Physical Oceanography, Woods Hole Oceanographic Institution, Mail Stop 21, 266 Woods Hole Road, Woods Hole, MA 02543-1050, USA.

C. Chen and G. W. Cowles, School for Marine Science and Technology, University of Massachusetts Dartmouth, New Bedford, MA 02744, USA.

D. B. Haidvogel, Institute of Marine and Coastal Science, Rutgers University, New Brunswick, NJ 08901, USA.

K. S. Hedstrom, Arctic Region Supercomputing Center, University of Alaska, Fairbanks, AK 99775, USA.

H. Huang, Department of Oceanography and Coastal Sciences, Louisiana State University, Baton Rouge, LA 70803, USA. (hhuang7@lsu.edu)

C. D. Winant, Scripps Institution of Oceanography, University of California, San Diego, La Jolla, CA 92093, USA.